



# Shear strength prediction of concrete beams reinforced with FRP bars using novel hybrid BR-ANN model

Trong-Ha Nguyen<sup>1</sup> · Xuan-Bang Nguyen<sup>2</sup> · Van-Hoa Nguyen<sup>1</sup> · Thu-Hang Thi Nguyen<sup>1</sup> · Duy-Duan Nguyen<sup>1</sup>

Received: 29 July 2023 / Accepted: 4 August 2023  
© The Author(s), under exclusive licence to Springer Nature Switzerland AG 2023

## Abstract

Shear strength is a very important parameter in designing of reinforced concrete beams or concrete beams reinforced with fiber-reinforced polymer (FRP) bars. So far, numerous studies and design codes have proposed empirical-based formulas for predicting the shear strength of FRP-concrete beams. However, a difference exists between the proposed formulas and experimental results. This study predicts the shear strength of FRP-concrete beams using the novel hybrid BR-ANN model, which integrates artificial neural network (ANN) and Bayesian regularization (BR). For that, a comprehensive database consisting of 303 experimental results is compiled for developing the BR-ANN models. The performance results of BR-ANN are compared with those of 15 existing empirical formulas, which were proposed in typical design codes and well-known published studies. The predicted outputs are evaluated utilizing indicators, which are goodness of fit ( $R^2$ ), root mean squared error (RMSE), and mean value of the ratio  $V_{\text{predict}}/V_{\text{test}}$ . The results reveal that the BR-ANN model outperforms other empirical formulas with a very high  $R^2$  (0.987), very small RMSE (7.3 kN). In addition, the mean value of the ratio  $V_{\text{predict}}/V_{\text{test}}$  is equal to unity. Moreover, effects of input variables on the shear strength are evaluated. Finally, a practical design tool is developed to apply the BR-ANN model in calculating the shear strength of FRP-concrete beams.

**Keywords** Artificial neural network (ANN) · Bayesian regularization (BR) · Concrete beam · Fiber-reinforced polymer (FRP) bar · Shear strength · Graphical user interface

## Introduction

Reinforced concrete (RC) beams are one of the critical members in buildings and bridges. The service life of RC structures has been gradually degraded due to due to corrosion

effects. Therefore, it is required to use non-corrosive materials as an alternative to conventional reinforcements.

Fiber-reinforced polymer (FRP) is one of potential solutions for reinforcing concrete structures due to its high resistance to corrosion and high strength to weight ratio (ACI, 2015; Askar et al., 2022; Xue et al., 2016). Overall, the mechanical properties of FRP are different from those of normal reinforcement. Thus, a comprehensive investigation on its behavior as a reinforced material is needed prior to its safe implementation in demanding structural applications. Shehata (1999) pointed out that the fundamental principles of flexural theories of conventional RC beams are also valid for concrete beams reinforced with longitudinal FRP bars. Nevertheless, because of its brittle failure mode, a higher material reduction factor should be used for design purposes when FRP bars used as reinforcements. Furthermore, the longitudinal FRP reinforcement contributes significantly to the nominal shear capacity of FRP-concrete beams. Similar conclusions were stated in other experimental studies (Bentz et al., 2010; Hoult et al., 2008).

✉ Duy-Duan Nguyen  
duan468@gmail.com

Trong-Ha Nguyen  
trongha@vinhuni.edu.vn

Xuan-Bang Nguyen  
nxb@lqdtu.edu.vn

Van-Hoa Nguyen  
vanhoakxd@vinhuni.edu.vn

Thu-Hang Thi Nguyen  
hang2391984@gmail.com

<sup>1</sup> Department of Civil Engineering, Vinh University,  
Vinh 461010, Vietnam

<sup>2</sup> Institute of Techniques for Special Engineering, Le Quy Don  
Technical University, Hanoi, Vietnam

Shear strength is one of the critical parameters in designing FRP-concrete beams. So far, numerous studies have been conducted to propose formulas for calculating the shear strength of the beams. Current design codes have provided the shear strength expressions for these beams such as ACI 440.1R (2015), AASHTO (2009), CNR-DT203 (2007), ISIS-M03 (2007), JSCE (1997), CSA S806 (2012), and BISE (1999). In addition, empirical formulas were developed by various researchers (Deitz et al., 1999; El-Sayed et al., 2006; Jumaa & Yousif, 2018; Kara, 2011; Marani & Nehdi, 2022; Michaluk et al., 1998; Nehdi et al., 2007; Tottori & Wakui, 1993; Tureyen & Frosch, 2002). Nevertheless, a discrepancy between calculated formulas and experiments is observed (Nehdi et al., 2007). Therefore, it is required to assess the shear strength provided by various models using extensive experimental data sets. Furthermore, a practical machine learning (ML)-based model should be developed for rapidly evaluating the shear strength of FRP-concrete beams without stirrups.

Artificial intelligence and ML techniques have been extensively applying in civil and structural engineering (Kaveh & Bondarabady, 2004; Kaveh & Servati, 2001; Kaveh et al., 2008; Nguyen et al., 2022; Tran & Nguyen, 2022). Artificial neural network (ANN) is one of the most powerful ML models that is using for predicting structural responses of RC structures (Ahmed et al., 2019; Asteris & Mokos, 2019; Kaveh & Khalegi, 1998; Kaveh & Khavanzadeh, 2023; Mai et al., 2022; Nguyen et al., 2021a, 2021b, 2021c; Rönnholm et al., 2005; Selvan et al., 2018; Tran et al., 2022; Tran & Kim, 2020; Vakhshouri & Nejadi, 2018). Moreover, some optimization techniques have been employed for improving performance of ANN models, such as Particle Swarm Optimization (PSO) (Eberhart & Kennedy, 1995; Nguyen et al., 2023b), Genetic algorithm (GA) (Nguyen et al., 2023a; Sivanandam et al., 2008), and Evolutionary optimization (Simon, 2013). Furthermore, Bayesian regularization (BR), which incorporates Bayesian inference and regularization techniques, is also widely used for preventing overfitting and improving prediction of neural networks (Burden & Winkler, 2009). An evaluation of applying the hybrid BR-ANN model for predicting shear strength of FRP-concrete beams is necessary.

Some studies have evaluated the shear strength of FRP-concrete beams using different ML models. Naderpour et al. (2018) used ANN to predict the shear strength of concrete beams reinforced with FRP bars. They compiled 110 tested data sets of FRP-concrete beams to train the ANN model with obtained  $R^2$  value of 0.93 and RMSE of 11.36 kN. Jumaa and Yousif (2018) predicted the shear capacity of FRP-concrete beams using ANN, GA, and regression analysis models. By collecting 269 databases, they emphasized that the performance of ANN was superior to others existing models with a high  $R^2$  of 0.987. In the study of Nikoo et al. (2021), ANN

optimized by bat algorithm was utilized for predicting the shear strength of FRP-concrete beams. A set of 140 data samples was used to develop the ML model, and they highlighted that the ML model was highly capable of calculating the shear capacity of the beams. Recently, Wakjira et al. (2022) developed various ML models for calculating the shear strength of FRP-RC beams. The ensemble ML models significantly outperformed other single ML and empirical models. Marani and Nehdi (2022) developed ML models to predict the shear capacity of FRP-RC beams, then proposed ML-based formula to calculate the shear strength of the beams. A high prediction performance was achieved with  $R^2$  of 0.96. In addition, their proposed equation showed an accuracy with  $R^2$  of 0.879 and RMSE of 23 kN. Previous studies developed various ML models for predicting the shear strength of FRP-concrete beams, however, an improvement of prediction models should be considered, and a practical tool for design engineers should be proposed.

The purpose of the present study is to develop a novel hybrid ML model for rapidly and accurately predicting the shear strength of FRP-concrete beams without stirrups. For that, a large database containing 303 test results are gathered from the literature. The predicted outputs are evaluated utilizing indicators, which are goodness of fit ( $R^2$ ), root mean squared error (RMSE), and mean value of the ratio  $V_{\text{predict}}/V_{\text{test}}$ . Performance of the hybrid ML model is then compared with that of 15 published formulas. Moreover, the influence of input parameters on the shear strength is thoroughly assessed. Finally, a convenient design tool for practical engineers is developed.

## Empirical models for shear strength calculations of FRP-concrete beams

In this study, we investigated 15 empirical formulas for calculating the shear strength of FRP-concrete beams, in which six equations in current design codes and nine published studies are considered. Six design codes include ACI 440.1R (2015), AASHTO (2009), CNR-DT203 (2007), ISIS-M03 (2007), JSCE (1997), and BISE (1999). Meanwhile, nice previously typical studies are Tottori and Wakui (1993), Michaluk et al. (1998), Deitz et al. (1999), Tureyen and Frosch (2002), El-Sayed et al. (2006), Nehdi et al. (2007), Kara (2011), Jumaa and Yousif (2018), and Marani and Nehdi (2022), as presented in Table 1.

## Database collection

An extensive database is gathered to develop the BR-ANN model for predicting shear strengths of FRP-concrete beams. A set of 303 experimental test results of FRP-concrete beams without stirrups are collected from the literature

**Table 1** Shear strength models of FRP-concrete beams without stirrups

Model	Expression
ACI 440.1R (2015)	$V = \frac{2}{5} b_w c \sqrt{f_c' t};$ (1) $c = kd; k = \sqrt{2\rho_f n + (\rho_f n)^2} - \rho_f n; n = \frac{E_f}{E_c}$ $b_w$ is the width of beam; $d$ is the effective depth of beam; $f_c'$ is the compressive strength of concrete; $E_f$ and $E_c$ are the elastic modulus of FRP bars and concrete, respectively
AASHTO (2009)	$V = (0.0676\sqrt{f_c'} t + 4.6\rho_f) b_w d \leq 0.126 b_w d \sqrt{f_c' t}$ (2)
CNR-DT203 (2007)	$V = 1.3 \left( \frac{E_f}{E_s} \right)^{0.5} \tau_{rd} k_d (1.2 + 40\rho_f) b_w d$ (3) $\tau_{rd} = 0.25 f_{ctk0.05}; f_{ctk0.05} = 0.7 f_{ctm}; f_{ctm} = (0.3 f_c')^{2/3};$ $k_d = 1.6 - d; E_s$ is the elastic modulus of reinforcement; $\rho_f$ is the FRP bar ratio
ISIS-M03 (2007)	$V = 0.2 b_w d \sqrt{f_c'} \left( \frac{E_f}{E_s} \right)^{0.5}$ for $d < 300$ mm; (4) $V = \frac{260}{1000+d} b_w d \sqrt{f_c'} \left( \frac{E_f}{E_s} \right)^{0.5} \leq 0.1 b_w d \sqrt{f_c'} \left( \frac{E_f}{E_s} \right)^{0.5}$ for $d \geq 300$ mm
JSCE (1997)	$V = \beta_d \beta_p \beta_n f_{vc} b_w d / \gamma_b;$ (5) $f_{vc} = 0.2 (f_c')^{1/3} \leq 0.72 \text{ MPa}; \beta_d = (1/d)^{0.25} \leq 1.5;$ $\beta_p = (100\rho_f E_f / E_s)^{1/3} \leq 1.5;$ $\beta_n = 1 + M_o / M_d \leq 2$ for $N_d \geq 0;$ $\beta_n = 1 + M_o / M_d \leq 2$ for $N_d < 0; \gamma_b = 1.3$
BISE (1999)	$V = 0.79 \left( 100\rho_f \frac{E_f}{E_s} \right)^{1/3} \left( \frac{400}{d} \right)^{1/4} \left( \frac{f_{cu}}{25} \right)^{1/3} b_w d; f_{cu} = 1.25 f_c'$ (6)
Tottori and Wakui (1993)	$V = 0.2 \left( 100\rho_f f_c' \frac{E_f}{E_s} \right)^{1/3} \left( \frac{d}{1000} \right)^{-1/4} \left[ 0.75 + \frac{1.4}{(a/d)} \right] b_w d$ (7)
Michaluk et al. (1998)	$V = \frac{E_f}{E_s} \left( \frac{1}{6} b_w d \sqrt{f_c'} \right)$ (8)
Deitz et al. (1999)	$V = 3 \frac{E_f}{E_s} \left( \frac{1}{6} b_w d \sqrt{f_c'} \right);$ (9) $k = \sqrt{2\rho_f n + (\rho_f n)^2} - \rho_f n; n = \frac{E_f}{E_c}$
Tureyen and Frosch (2002)	$V = \frac{5}{12} k \frac{E_f}{E_s} \left( b_w d \sqrt{f_c'} \right)$ (10)
El-Sayed et al. (2006)	$V = \left( \frac{\rho_f E_f}{90\beta_1 E_s f_c'} \right)^{1/3} \left( \frac{\sqrt{f_c'}}{6} b_w d \right) \leq \frac{\sqrt{f_c'}}{6} b_w d;$ (11) $\beta_1 = 0.85 - 0.05 \left( \frac{f_c' t - 28}{7} \right) \geq 0.65$
Nehdi et al. (2007)	$V = 2.1 \left( \frac{f_c' \rho_f d}{a} \frac{E_f}{E_s} \right)^{0.3}$ for $a/d > 2.5$ (12) $V = 2.5 \frac{d}{a} 2.1 \left( \frac{f_c' \rho_f d}{a} \frac{E_f}{E_s} \right)^{0.3}$ for $a/d < 2.5;$ $a/d$ is the shear span
Kara (2011)	$V = b_w d \left( \sqrt[3]{\frac{d}{a}} f_c' \rho_f \frac{E_f}{E_s} (c_1^2/c_0) \right)^{1/3} c_0/c_2;$ (13) $c_0 = 7.696; c_1 = 7.245; c_2 = 7.718$
Jumaa and Yousif (2018)	$V = 0.32 \left( \frac{1}{d} \right)^{1/3} \left( \frac{E_f \rho_f}{a/d} \right)^{2/5} (f_c')^{1/5} b_w d$ (14)
Marani and Nehdi (2022)	$V = 2.35 (f_c')^{0.5} \rho_f^{0.2} \left( \frac{d}{a} \frac{E_f}{E_s} \right)^{0.333} b_w^{0.9} d^{0.9}$ (15)

(Peng et al., 2020). It should be again noted that  $b_w$  is the width of beam;  $d$  is the effective depth of beam;  $a/d$  is the shear span to effective depth ratio;  $a$  is the shear span;  $f_c'$

is the compressive strength of concrete;  $E_f$  and  $E_c$  are the elastic modulus of FRP bars and concrete, respectively;  $\rho_f$  is the FRP bar ratio;  $V$  is the shear strength.

It should be noted that the collected database considers only simply supported slender beams (i.e.,  $a/d \geq 2.5$ ). Among 303 specimens, there are 294 rectangular beams, and the remaining ones are I- and T-section beams. In addition, 208 beams were reinforced with carbon FRP bars. Only the shear failure mode of the FRP-concrete beams is retained in the data. Figure 1 depicts the FRP-concrete beams without stirrups. Table 2 describes statistically collected data samples. The frequencies of the database are demonstrated in Fig. 2. Furthermore, the interrelationship between the parameters of database is summarized in Fig. 3. A description of all 303 data sets is provided in the Appendix.

## Bayesian regularized of artificial neural network (BR-ANN)

### Theoretical backgrounds

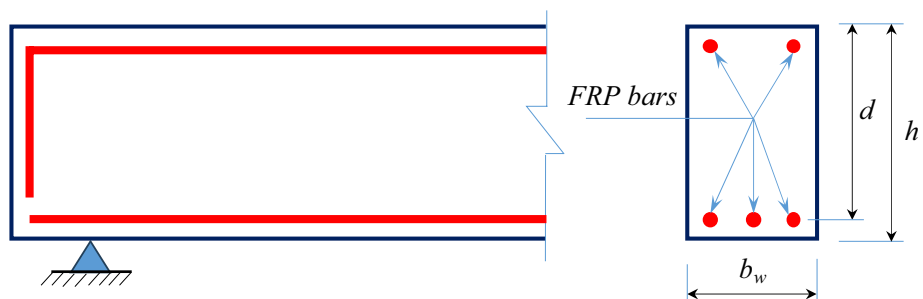
ANNs have been widely used to resolve different structural engineering problems. Neurons (nodes) are the basic building blocks of an ANN that are artificial neurons or nodes. These nodes receive inputs, perform computations, and predict outputs. They are organized into layers. The three main types of layers in an ANN: (1) input layer, (2) hidden layers, and (output layer). Connections between neurons represent the strength of the relationship between them. Each connection is associated with a weight ( $w_i$ ), which determines the impact of the input on the output of the neuron. Backpropagation is a key algorithm used to train and update the weights of ANNs. It is a form of supervised learning that adjusts the weights in the network based on the error between the predicted output and the actual output. Figure 4

shows the ANN structure and used activation functions. The main steps of how the backpropagation algorithm works in an ANN model include:

- (1) *Forward propagation* In the forward propagation step, the input data are passed through the network, layer by layer, to produce a predicted output. Each neuron applies an activation function to the weighted sum of its inputs and passes the result to the next layer.
- (2) *Calculate error* After the forward propagation, the predicted output is compared to the actual output using a loss function. The error is calculated as the difference between the predicted output ( $Y_i$ ) and the true output.
- (3) *Backpropagation of error* Starting from the output layer, the error is propagated backward through the network. The goal is to distribute the error among the neurons in the previous layers, proportionally to their contribution to the overall error.
- (4) *Update weights* As the error is propagated backward, the weights of the connections between neurons are updated to minimize the error.
- (5) *Repeat steps 1–4* The forward propagation, error calculation, backpropagation, and weight updates are repeated for multiple iterations or epochs until the model converges or reaches a stopping criterion, such as a maximum number of iterations or a desired level of performance.

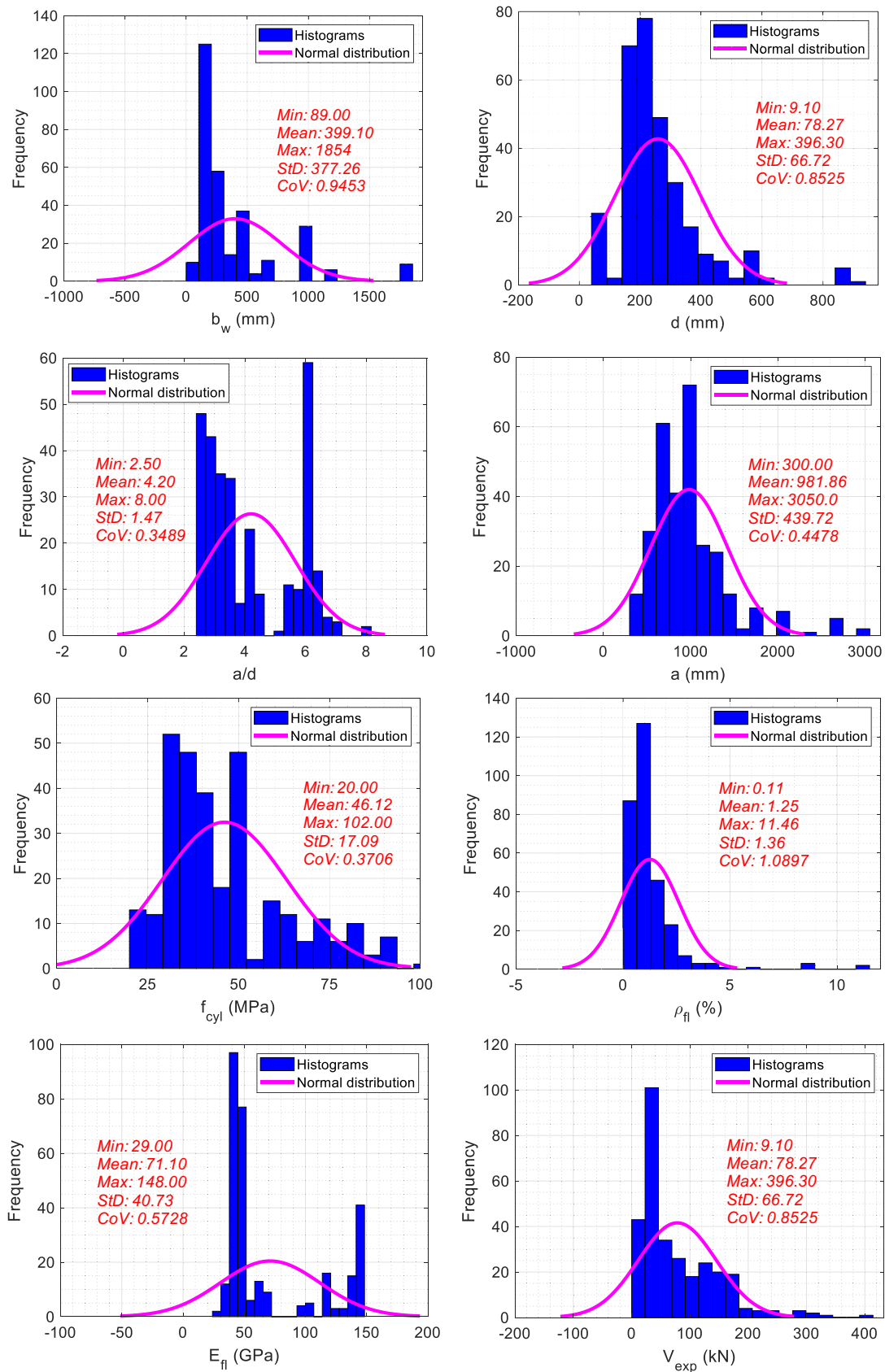
Backpropagation allows the ANN model to learn and adjust the weights based on the errors made during the prediction process. By iteratively updating the weights, the model gradually improves its ability to make accurate predictions. It is worth noting that backpropagation is just one part of the

**Fig. 1** Concrete beams reinforced with FRP bars without stirrups



**Table 2** Summary of used database

	$b_w$ (mm)	$d$ (mm)	$a/d$	$a$ (mm)	$f_c'$ (MPa)	$\rho_l$ (%)	$E_f$ (GPa)	$V$ (kN)
Max	1854	937	8	3050	102	11.46	148	396.3
Mean	399	258	4	982	46	1	71	78
Min	89	73	2.5	300	20	0.11	29	9.1
SD	377	141	1	440	17	1	41	67
COV	0.95	0.55	0.35	0.45	0.37	1.09	0.57	0.85

**Fig. 2** Histograms of used database

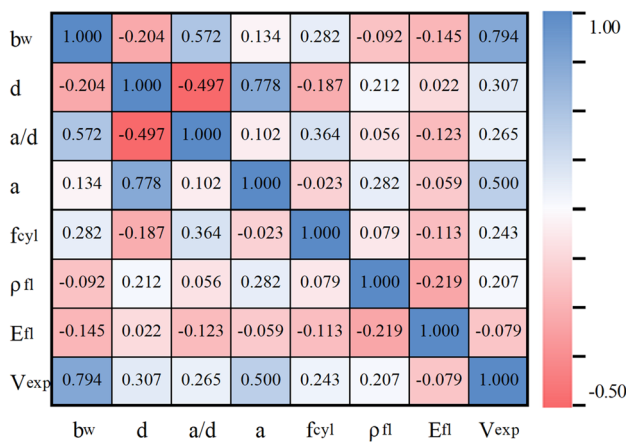
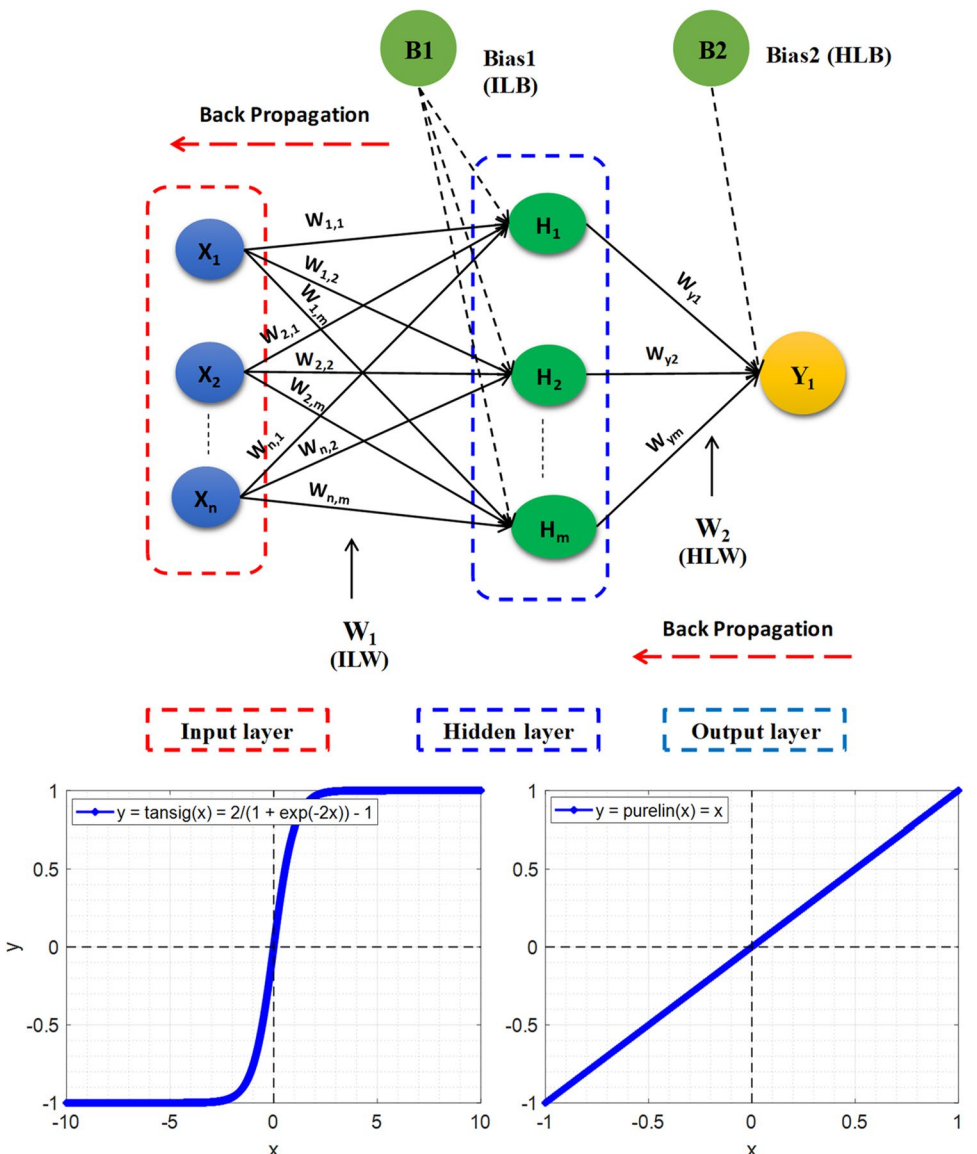


**Fig. 3** Pearson's correlations of parameters in the database

**Fig. 4** ANN structure and used activation functions



overall training process for ANNs. Other techniques, such as regularization, dropout, and learning rate scheduling, are often used in combination with backpropagation to further improve the model's performance and prevent overfitting.

In this study, Bayesian regularization algorithm is used to improve the performance of ANNs. The essence of BR-ANN is to optimize the objective function  $F(w)$ , which is expressed by Eq. (16):

$$F(w) = \beta E_D + \alpha E_w \quad (16)$$

$$E_D = \frac{1}{N} \sum_i^N (y_i - t_i)^2 = \frac{1}{N} \sum_i^N e_i^2 \quad (17)$$

$$E_w = \frac{1}{2} \sum_i^m w_i^2, \quad (18)$$

where  $E_D$  and  $E_w$  are the mean squared error and mean squared weight, respectively;  $\alpha$  and  $\beta$  are hyperparameters;  $w$  and  $m$  are weight and number of weights, respectively;  $D(x_i, t_i)$  is the training data;  $y_i$  is the  $i$ -th output corresponding to the  $i$ -th training set.

For BR-ANN, the initiated weights are random values. According to Bayes' theorem, the density function  $P(w|D, \alpha, \beta, M)$  for weights can be determined by Eq. (19).

$$P(w|D, \alpha, \beta, M) = \frac{P(D|w, \beta, M)P(w|\alpha, M)}{P(D|\alpha, \beta, M)}, \quad (19)$$

where  $M$  is the ANN structure;  $P(w|\alpha, M)$  and  $P(D|w, \beta, M)$  are the prior density and the likelihood functions, respectively. During training data sets, weights are assumed to be interference variables in the Gaussian distribution, the probability densities of  $P(w|\alpha, M)$  and  $P(D|w, \beta, M)$  are determined as follows.

$$P(D|w, \beta, M) = \frac{1}{Z_D(\beta)} \exp(-\beta E_D) = \left(\frac{\pi}{\beta}\right)^{-\frac{N}{2}} \exp(-\beta E_D) \quad (20)$$

$$P(w|\alpha, M) = \frac{1}{Z_w(\alpha)} \exp(-\alpha E_w) = \left(\frac{\pi}{\alpha}\right)^{-\frac{m}{2}} \exp(-\alpha E_w). \quad (21)$$

Substituting Eqs. (20) and (21) into Eq. (19), the probability density function  $P(w|D, \alpha, \beta, M)$  can be re-written as

$$\begin{aligned} P(w|D, \alpha, \beta, M) &= \frac{\frac{1}{Z_D(\beta)} \cdot \frac{1}{Z_w(\alpha)} \exp(-(\beta E_D + \alpha E_w))}{P(D|\alpha, \beta, M)} \\ &= \frac{1}{Z_F(\alpha, \beta)} \exp(-F(w)), \end{aligned} \quad (22)$$

where

$$\alpha = \frac{\gamma}{2E_w}; \beta = \frac{N - \gamma}{2E_D}; \gamma = N - 2\alpha \text{tr}(H)^{-1}.$$

According to Foresee and Hagan (1997), Hessian matrix  $H$  is calculated using the Gauss–Newton approximation of Levenberg–Marquardt (LM) algorithm, expressed by

$$H = \nabla^2 F(w) \approx 2\beta J^T J + 2\alpha I_N. \quad (23)$$

In the BR-ANN technique, optimizing weights is associated with maximizing the function  $P(w|D, \alpha, \beta, M)$  or minimizing the objective function  $F(w)$ . LM algorithm is iterated until a minimum convergence of  $F(w)$  is obtained. The weights can be calculated by

$$w_{i+1} = w_i (J_i^T J_i + \mu_i I)^{-1} J_i^T e_i, \quad (24)$$

where  $J$  is the Jacobian matrix for the training error.

The basic steps for performing BR-ANN model are as follows:

- (1) Initialize the weights and biases for the neural network.
- (2) Define the likelihood function as the probability of the output given the input and the current weights and biases.
- (3) Define the prior distribution over the weights.
- (4) Choose a regularization coefficient.
- (5) Choose a validation set for tuning hyperparameters.
- (6) For each epoch:
  - Shuffle the training data.
  - Forward propagate the input through the network.
  - Compute the likelihood and the prior.
- (7) Posterior probability with regularization.
  - Backpropagate the errors to obtain the gradient of the weights and biases.
  - Update the weights and biases using gradient descent.
  - Evaluate the performance on the validation set and update the hyperparameters if necessary.
- (8) After training, evaluate the performance of the neural network on a separate test set.
- (9) Save the weights and biases for future use.

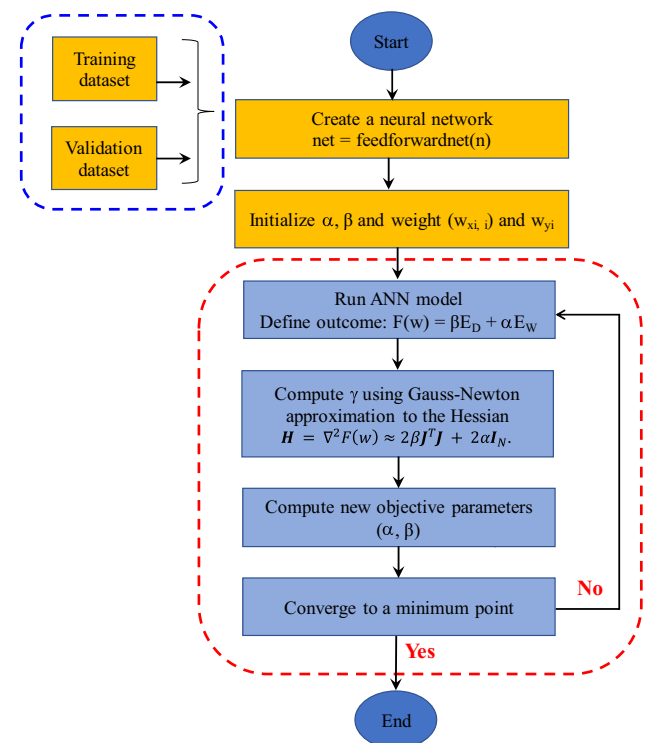


**Fig. 5** Flowchart of BR-ANN

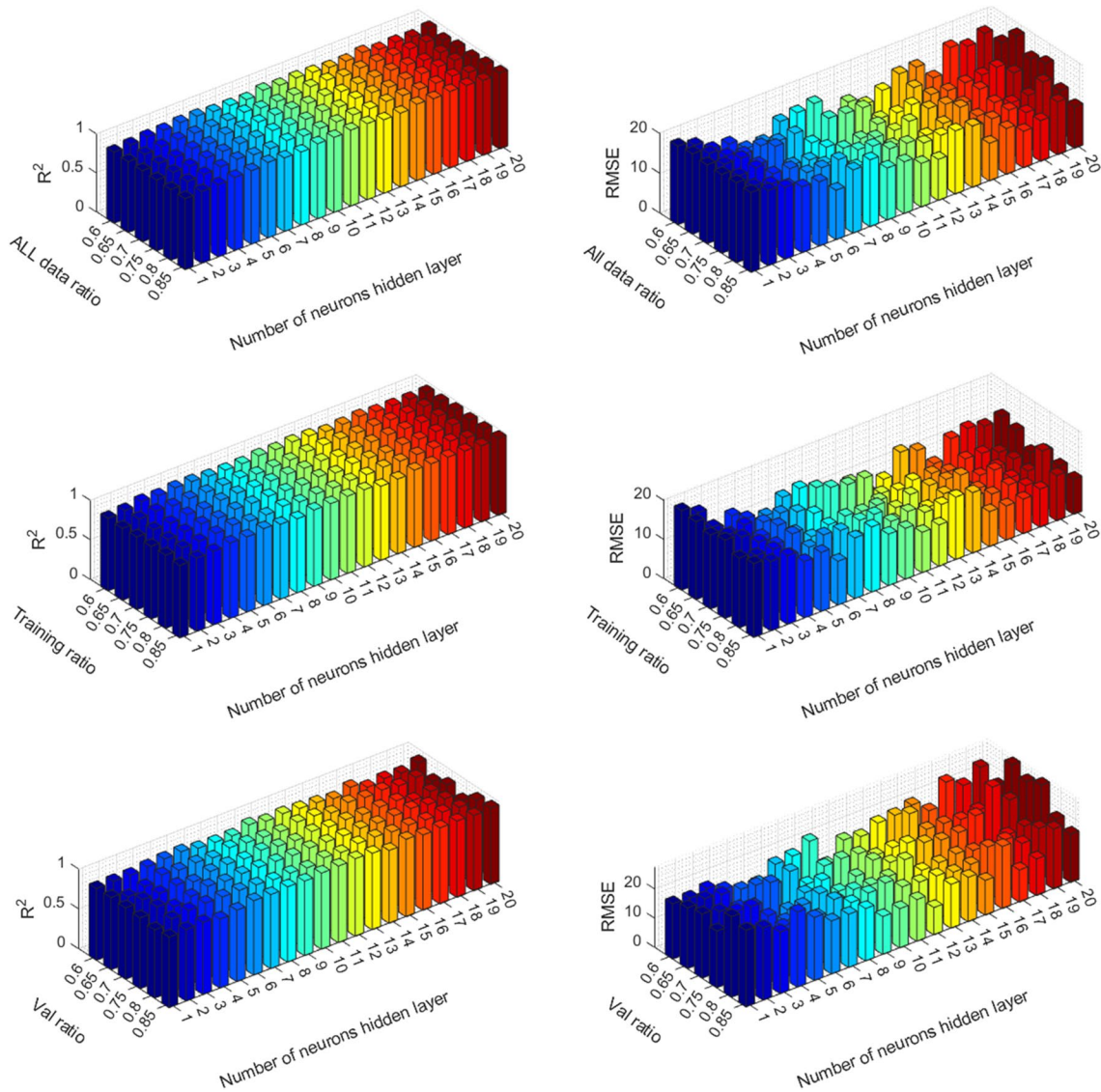


**Fig. 6** Performance of 120 ANN models

The flowchart of BR-ANN is shown in Fig. 5.

### Performance metrics

In this study, statistical parameters, which are  $R^2$  and RMSE are employed to evaluate the accuracy of predictive models including BR-ANN and 15 shear strength formulas in Table 1. It should be noted that the  $R^2$  is a statistical concept that measures how well a calculated set of data matches an experimental result. In other words, it evaluates how well the data fit the empirical model being used to predict the experiment. The higher the  $R^2$  is, the better performance of the calculated shear model. Meanwhile,

RMSE is a commonly used statistical metric that measures the difference between predicted values and observed values. It is the square root of the average of the squared differences between the predicted and actual values. RMSE is often used to evaluate the accuracy of a predictive model, such as in regression analysis, and is a measure of how well the model fits the data. The lower the RMSE, the better the model is at predicting the outcome variable. The expressions of  $R^2$  and RMSE are described in following equations:

$$R^2 = 1 - \left( \frac{\sum_{i=1}^N (t_i - o_i)^2}{\sum_{i=1}^N (t_i - \bar{o})^2} \right) \quad (25)$$

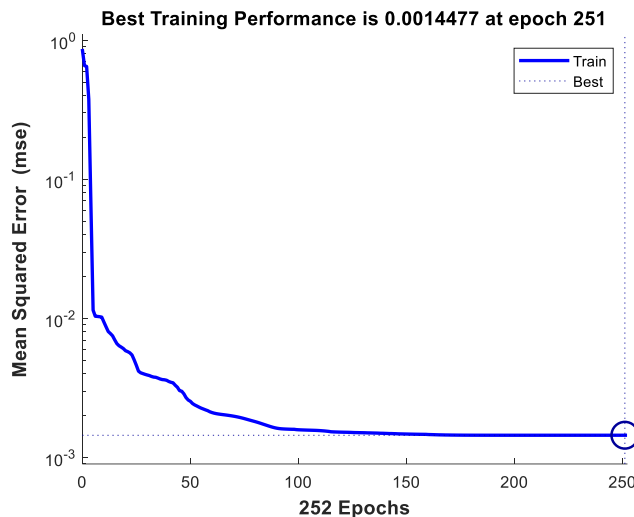


**Fig. 7** Convergence of training BR-ANN

**Table 3** Performance metrics of BR-ANN model

Data set	$R^2$	RMSE (kN)	$V_{\text{predict}}/V_{\text{test}}$		
			Mean	SD	CoV
All data	0.987	7.366	1.00	0.116	0.115
Training	0.987	7.069	1.01	0.114	0.113
Validation	0.989	8.442	1.00	0.124	0.123

$$\text{RMSE} = \sqrt{\left(\frac{1}{n}\right) \sum_{i=1}^n (t_i - o_i)^2}, \quad (26)$$

where  $t_i$  and  $o_i$  represent the target and output of  $i$ th data point, respectively;  $\bar{o}$  is the mean of output data samples;  $N$  is the number of samples.

## Results and discussion

### Performance of BR-ANN

For obtaining the most efficient ANN model, we tested 120 structures with various portions of training data including 0.6, 0.65, 0.7, 0.75, 0.8, and 0.85, whereas the validating data were taken the remaining. Moreover, the effects of the number of neurons in the hidden layer were investigated by changing from 1 up to 20.  $R^2$  and RMSE were quantified to evaluate those models, as demonstrated in Fig. 6. Consequently, the best model was chosen with the highest  $R^2$  and smallest RMSE.

The selected ANN model with 70% training data and 7 neurons in the hidden layer was retained for constructing the hybrid BR-ANN model. The convergence of training BR-ANN model was achieved after 251 epochs with a very small mean square error (MSE) of 0.0014477 (i.e., almost zero). In addition, the regression performance of BR-ANN model is shown in Fig. 7, and performance metrics are provided in

**Fig. 8** Regression performance of BR-ANN model

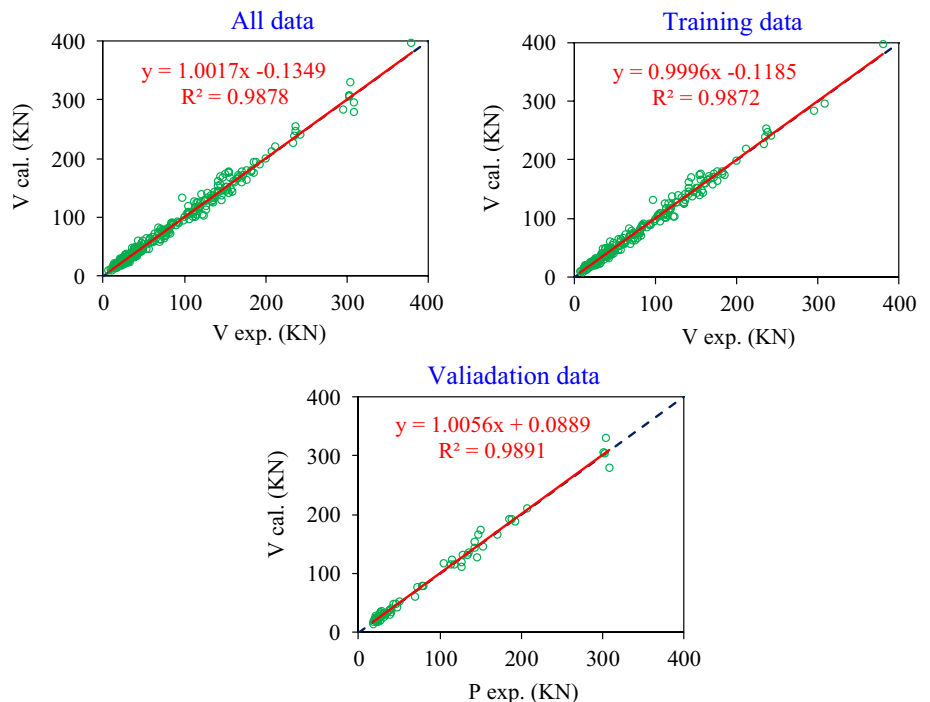


**Fig. 9** Comparison of performance between BR-ANN model and existing formulas

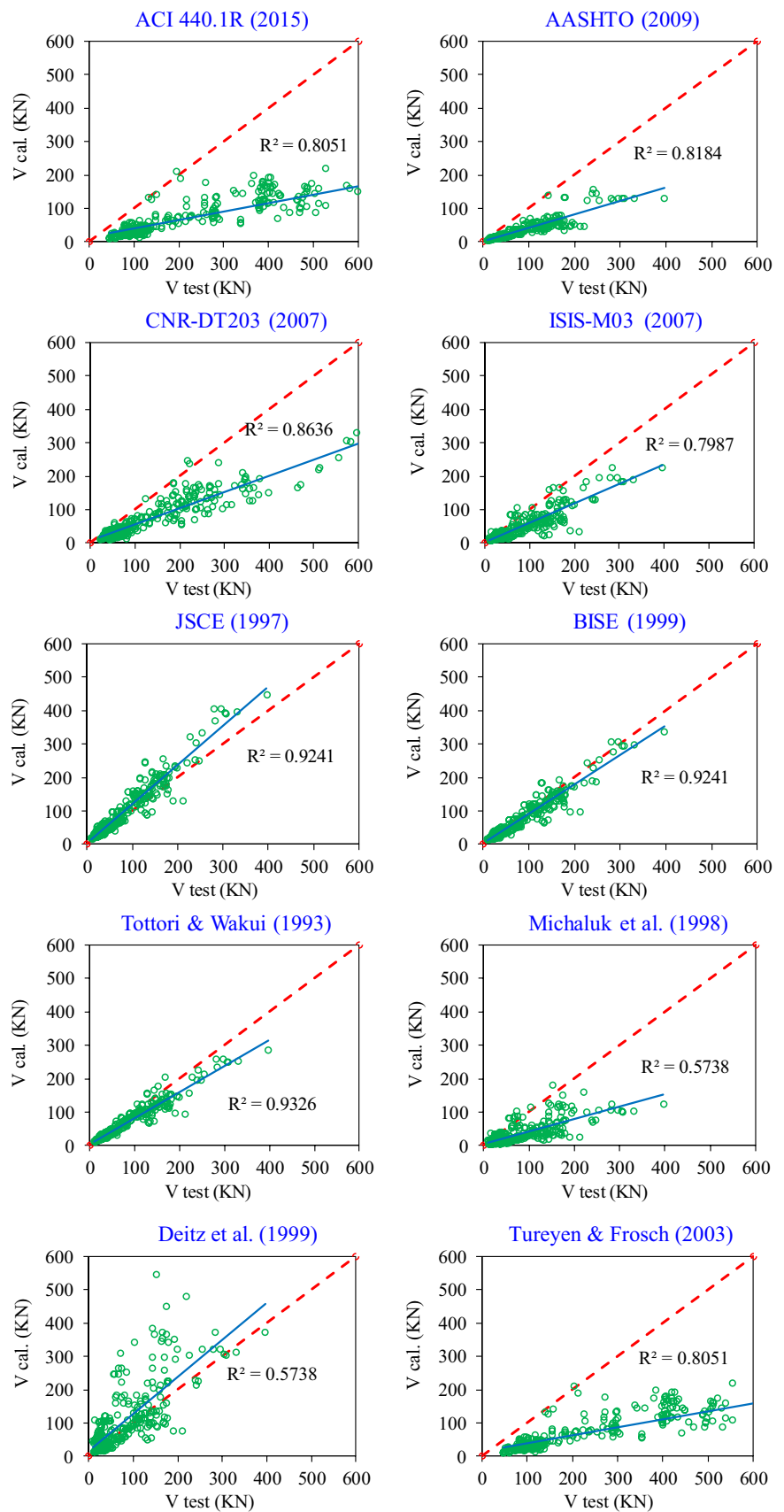


Fig. 9 (continued)

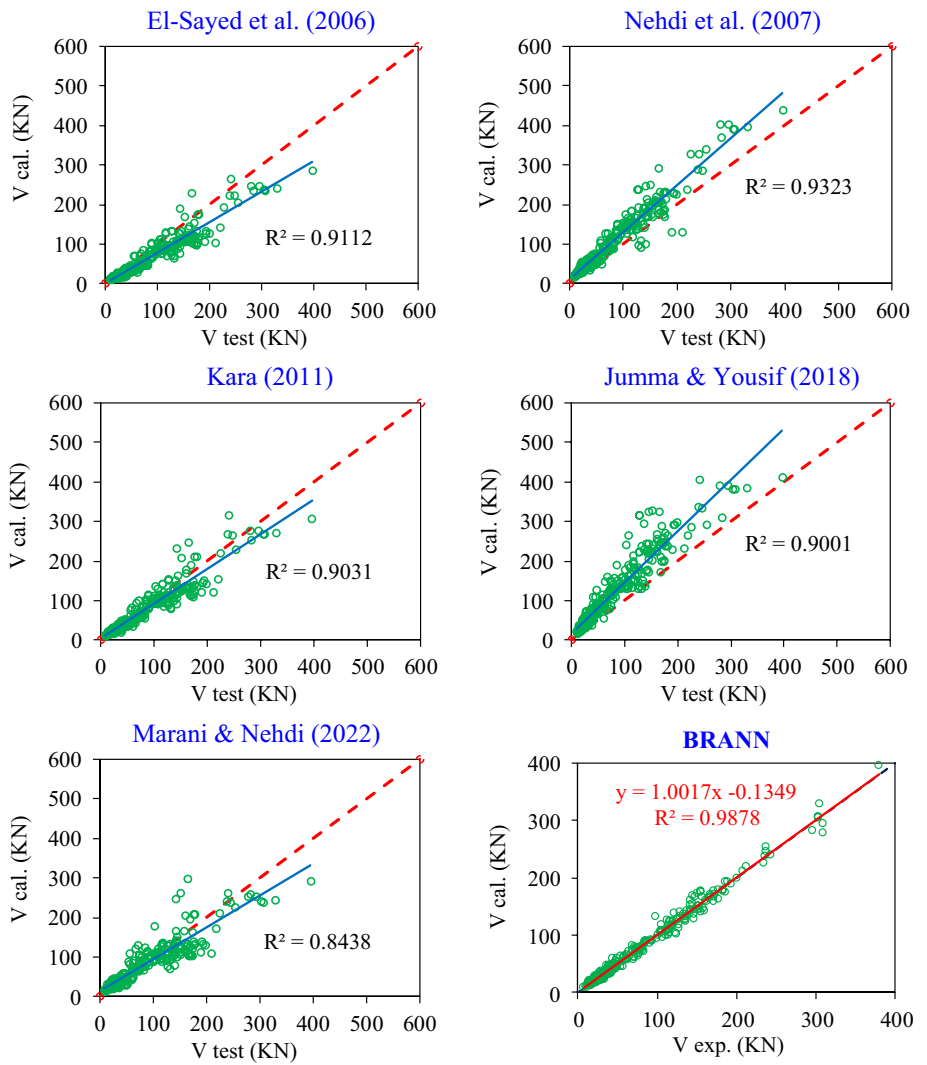


Table 3. It was found that  $R^2$  and RMSE values were mostly 0.99 and 7.3 kN for all data sets, respectively. The mean of the ratio  $V_{\text{predict}}/V_{\text{test}}$  was 1.0. Those results indicated that the ML model achieved a highly accurate prediction (see Fig. 8).

### Comparison of predicted results between BR-ANN and existing formulas

Figure 9 shows the comparison of performance between BR-ANN model and 15 existing formulas for calculating shear strength of FRP-concrete beams. It should be noted that the dash red line is the 1:1 line, meanwhile the solid blue line is the linear regression. It is found that BR-ANN showed to be the most accurate model, followed by Tottori and Wakui (1993), BISE (1999), and Kara (2011). In addition, the predicted models proposed by El-Sayed et al. (2006) and Marani and Nehdi (2022) had a good performance with high  $R^2$  values and the linear regressions were relatively close to

the 1:1 line. In addition, the results of these formulas were close to the experiments and slightly conservative compared to the other formulas. Moreover, calculated shear strengths of Nehdi et al. (2007), JSCE (1997), and Jumaa and Yousif (2018) were also close to the experiment results, but their results had a trend being larger than that of the test ones. On the other hand, the results of ACI440.1R (2015), CNR-DT203 (2007), Tureyen and Frosch (2002), Michaluk et al. (1998), and AASHTO (2009) showed to be significantly conservative compared with the experimental tests.

Table 4 shows the calculated statistical indicators, which are  $R^2$  and RMSE, obtained from various predictive models. In addition, the properties of the ratio,  $V_{\text{predict}}/V_{\text{test}}$ , were evaluated, in which mean, standard deviation (SD), and coefficient of variation (CoV) were quantified. The results highlighted that BR-ANN was the most efficient model with the highest  $R^2$  value of 0.987 and the smallest RMSE of 7.3 kN. Moreover, the mean value of  $V_{\text{predict}}/V_{\text{test}}$  is equal to 1.0, implying that the ML model predicted accurately. It was also observed that

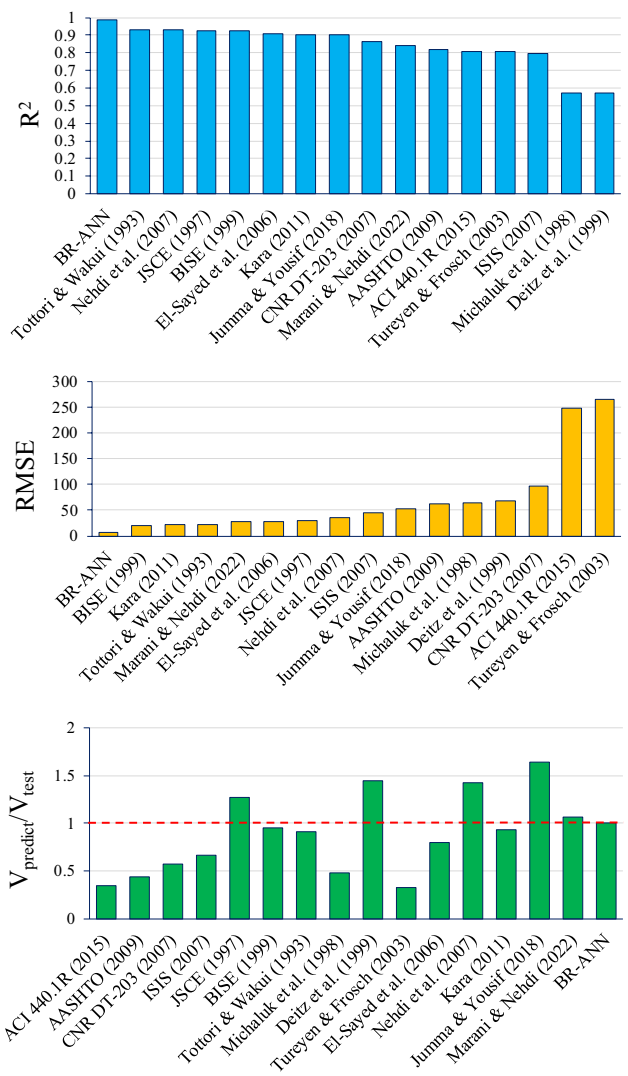
**Table 4** Statistical indicators for evaluating shear strength models of FRP-concrete beams

Model	$R^2$	RMSE (kN)	Statistical properties of $V_{\text{predict}}/V_{\text{test}}$		
			Mean	SD	CoV
ACI 440.1R (2015)	0.805	248	0.34	0.13	0.318
AASHTO (2009)	0.818	62	0.44	0.12	0.27
CNR-DT203 (2007)	0.863	97	0.57	0.17	0.292
ISIS (2007)	0.798	46	0.66	0.27	0.41
JSCE (1997)	0.924	30	1.27	0.29	0.23
BISE (1999)	0.924	20	0.95	0.22	0.23
Tottori and Wakui (1993)	0.932	23	0.91	0.18	0.20
Michaluk et al. (1998)	0.573	65	0.48	0.33	0.68
Deitz et al. (1999)	0.573	69	1.45	0.99	0.68
Tureyen and Frosch (2002)	0.805	265	0.32	0.12	0.380
El-Sayed et al. (2006)	0.911	28	0.80	0.17	0.21
Nehdi et al. (2007)	0.932	35	1.42	0.29	0.20
Kara (2011)	0.903	22	0.93	0.19	0.20
Jumma and Yousif (2018)	0.900	53	1.64	0.36	0.22
Marani and Nehdi (2022)	0.843	27	1.06	0.30	0.28
BR-ANN	0.987	7.3	1.00	0.116	0.115

Tottori and Wakui (1993), BISE (1999), Kara (2011), El-Sayed et al. (2006), and Marani and Nehdi (2022) provided a good performance. Furthermore, the formulas of Marani and Nehdi (2022), JSCE (1997), and Jumma and Yousif (2018) yield high  $R^2$  values (0.932, 0.924, and 0.90, respectively) and the medium RMSE (35 kN, 30 kN, 53 kN, respectively). However, mean values of  $V_{\text{predict}}/V_{\text{test}}$  of these models are larger than 1.0 (1.42, 1.27, 1.64, respectively), indicating an over-estimation. Meanwhile, the results of ACI440.1R (2015), CNR-DT203 (2007), Tureyen and Frosch (2002), Michaluk et al. (1998), and AASHTO (2009) had a large discrepancy compared to the experimental results. The ranking of different models using  $R^2$ , RMSE, and mean values of  $V_{\text{predict}}/V_{\text{test}}$  is shown in Fig. 10. Once again, it is very easy to recognize that the BR-ANN model outperformed empirical formulas.

## Sensitivity analysis

To quantify the effects of input design parameters on the calculated shear strength of FRP-concrete beams, sensitivity analyses should be conducted. It is noted that when considering the sensitivity of one specific parameter other

**Fig. 10** Comparison of performance indicators between various predictive models

parameters were set at the mean values. Figure 11 shows the effects of input parameters on the predicted shear strength of FRP-concrete beams. It can be found that the shear strength  $V$  was significantly increased with an increment of  $b_w$ ,  $d$ , and  $\rho_f$ . In other words, these parameters have positively affected the shear strength of the beams. Meanwhile, the shear span ( $a$ ) had a negative effect on the calculated result. Moreover, the compressive strength of concrete and elastic modulus of FRP bars insignificantly influences the predicted shear strength. The last sub-figure also demonstrates the ranking of important features, in

**Fig. 11** Effects of input parameters on predicted shear strength of FRP-concrete beams

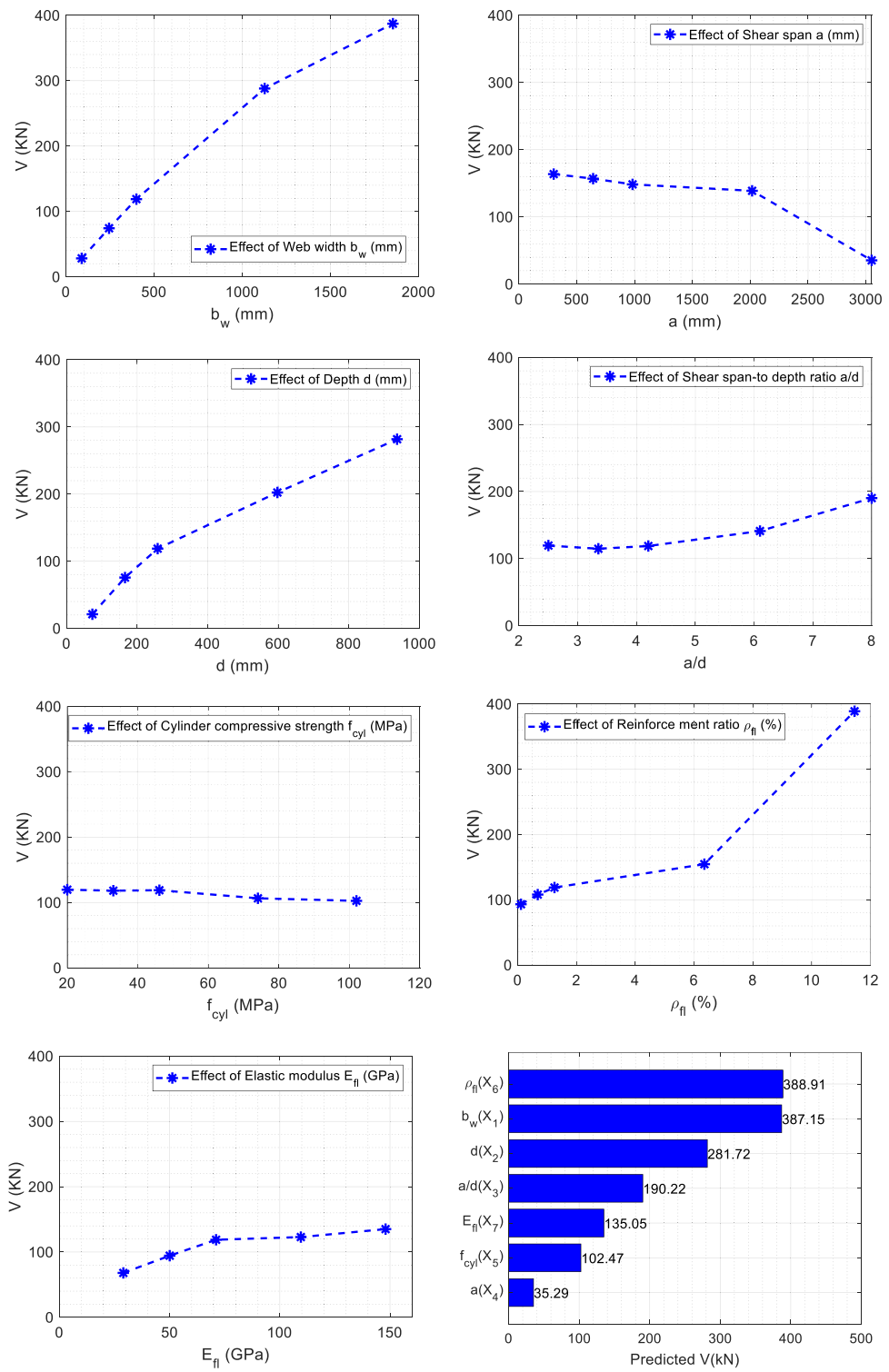
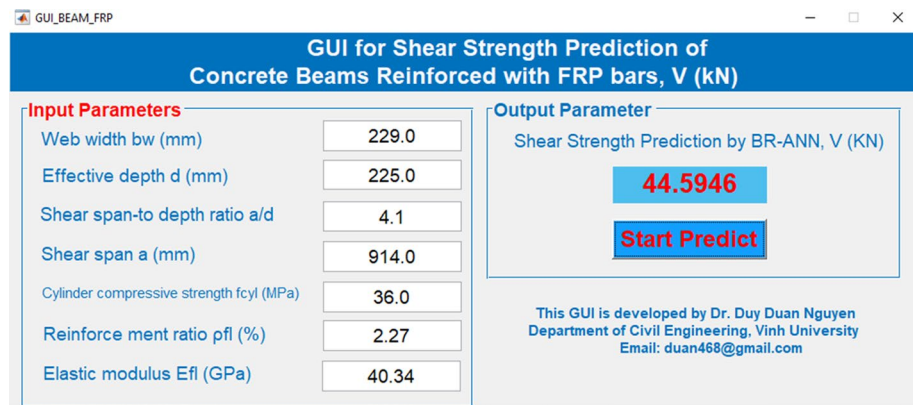


**Fig. 12** Practical GUI tool for shear strength of FRP-concrete beams



which  $\rho_f$  and  $b_w$  are the most important parameters, followed by the effective depth of beam ( $d$ ).

### Practical GUI program

For applying the BR-ANN model for design purposes, a practical tool such as graphical user interface (GUI) or mathematical equation should be proposed. This study developed a GUI tool for simplifying the design process of FRP-concrete beams. Figure 12 shows the proposed GUI tool in calculating the shear strength of the beam. It should be noted that this tool is convenient for use, and it is provided freely at this source: [https://github.com/duyduan1304/GUI\\_FRP-concrete-beams](https://github.com/duyduan1304/GUI_FRP-concrete-beams).

### Conclusions

This study developed a hybrid BR-ANN model for predicting shear strength of FRP-concrete beams without stirrups. An extensive database including 303 experimental test results of FRP-concrete beams was collected. The predicted performance of BR-ANN was compared with that of 15 empirical formulas, which were proposed in six design codes and nine published studies. The calculated accuracy of predictive models was assessed using statistical indicators, which were  $R^2$ , RMSE, and the mean value of ratio  $V_{\text{predict}}/V_{\text{test}}$ . The main conclusions are drawn as follows.

- The hybrid BR-ANN model outperforms other empirical formulas with a very high  $R^2$  (0.987) and very small RMSE (7.3 kN). In addition, the mean value of the ratio  $V_{\text{predict}}/V_{\text{test}}$  is equal to unity.
- The width of beam ( $b_w$ ), effective depth of beam ( $d$ ), and FRP ratio ( $\rho_f$ ) are the most influential parameters on shear strength of FRP-concrete beams. Meanwhile, the shear span ( $a$ ) had a negative effect on the calculated result. Moreover, the compressive strength of concrete

( $f_c'$ ) and elastic modulus of FRP bars ( $E_f$ ) insignificantly influence the predicted shear strength.

- A practical GUI tool is developed to apply the BR-ANN model in calculating the shear strength of FRP-concrete beams.

### Appendix. The used database

ID	$b_w$ (mm)	$d$ (mm)	$a/d$	$a$ (mm)	$f_c'$ (MPa)	$\rho_f$ (%)	$E_f$ (GPa)	$E_c$ (MPa)	$V$ (kN)
1	229	225	4.1	914	36	1.11	40.34	20	39.1
2	178	225	4.1	914	36	1.42	40.34	20	32.5
3	229	225	4.1	914	36	1.65	40.34	20	45.4
4	279	225	4.1	914	36	1.81	40.34	20	46.5
5	254	225	4.1	914	36	2.05	40.34	20	46.2
6	229	225	4.1	914	36	2.27	40.34	20	43.2
7	1000	165	6.06	1000	40	0.39	114	20	143.8
8	1000	165	6.06	1000	40	0.78	114	20	170.8
9	1000	161	6.21	1000	40	1.17	114	20	193.8
10	1000	162	6.17	1000	40	0.86	40	20	116.8
11	1000	159	6.29	1000	40	1.7	40	20	145.8
12	1000	162	6.17	1000	40	1.71	40	20	166.8
13	1000	159	6.29	1000	40	2.44	40	20	166.8
14	1000	154	6.49	1000	40	2.63	40	20	171.8
15	250	326	3.07	1000	50	0.87	128	20	79.7
16	250	326	3.07	1000	50	0.87	39	20	72.7
17	250	326	3.07	1000	45	1.24	134	20	106.2
18	250	326	3.07	1000	45	1.22	42	20	62.2
19	250	326	3.07	1000	44	1.72	134	20	126.7
20	250	326	3.07	1000	44	1.71	42	20	79.7
21	250	326	3.07	1000	63	1.71	135	20	132.2
22	250	326	3.07	1000	63	1.71	42	20	89.2
23	250	326	3.07	1000	63	2.2	135	20	176.2
24	250	326	3.07	1000	63	2.2	42	20	117.7
25	600	262	6.68	1750	68	0.77	48	20	89.2
26	600	262	6.68	1750	68	1.53	48	20	116.2

ID	$b_w$ (mm)	$d$ (mm)	$a/d$	$a$ (mm)	$f_c'$ (MPa)	$\rho_l$ (%)	$E_f$ (GPa)	$E_c$ (MPa)	$V$ (kN)	ID	$b_w$ (mm)	$d$ (mm)	$a/d$	$a$ (mm)	$f_c'$ (MPa)	$\rho_l$ (%)	$E_f$ (GPa)	$E_c$ (MPa)	$V$ (kN)
27	150	180	3.7	667	28	0.45	38	20	13	77	200	220	2.5	550	30	0.32	48.2	20	25.7
28	150	220	3.03	667	28	0.71	32	20	18.1	78	150	220	2.5	550	30	0.43	48.2	20	24.4
29	150	240	2.78	667	28	0.86	32	20	25.8	79	150	220	2.5	550	30	0.77	49.1	20	27.3
30	150	180	3.7	667	49	1.39	32	20	18	80	200	220	3.5	770	30	0.32	48.2	20	27.2
31	150	220	3.03	667	49	1.06	32	20	28.1	81	150	220	3.5	770	30	0.43	48.2	20	21.1
32	150	240	2.78	667	49	1.15	32	20	30.8	82	150	220	3.5	770	30	0.77	49.1	20	19.5
33	457	360	3.4	1219	35	0.96	40.54	20	108.1	83	200	220	4.5	990	30	0.32	48.2	20	20
34	457	360	3.4	1219	35	0.96	37.88	20	94.7	84	150	220	4.5	990	30	0.43	48.2	20	17.2
35	457	360	3.4	1219	35	0.96	47.1	20	114.8	85	150	220	4.5	990	30	0.77	49.1	20	20.5
36	457	360	3.4	1219	35	1.92	40.54	20	137	86	200	220	3	660	34	0.32	146.2	20	26.2
37	457	360	3.4	1219	35	1.92	37.88	20	152.6	87	150	220	3	660	34	0.43	146.2	20	19.2
38	457	360	3.4	1219	35	1.92	47.1	20	177	88	200	220	3	660	40	0.32	146.2	20	23.6
39	200	225	2.67	600	41	0.25	145	20	37	89	150	220	3	660	40	0.43	146.2	20	21.4
40	200	225	2.67	600	49	0.5	145	20	47.9	90	150	220	3	660	40	0.77	147.9	20	26.5
41	200	225	2.67	600	41	0.63	145	20	48.1	91	200	220	3	660	34	0.32	48.2	20	21.1
42	200	225	2.67	600	41	0.88	145	20	43.6	92	150	220	3	660	34	0.43	48.2	20	18.9
43	200	225	3.56	800	41	0.5	145	20	47.8	93	200	220	3	660	40	0.32	48.2	20	20.8
44	200	225	4.5	950	41	0.5	145	20	39.2	94	150	220	3	660	40	0.43	48.2	20	20.3
45	150	250	3	750	34	1.51	105	20	45.6	95	150	220	3	660	40	0.77	49.1	20	21.8
46	150	250	3	750	34	3.02	105	20	46.6	96	150	223	3.3	750	40	1.1	45	20	27.9
47	150	250	3	750	34	2.27	105	20	41.1	97	457	883	3.1	2743	30	0.6	41	20	179.6
48	178	279	2.69	750	24	2.3	40	20	54	98	457	883	3.1	2743	30	0.6	41	20	176.9
49	178	287	2.61	750	24	0.77	40	20	36.6	99	114	292	3.1	914	32	0.6	43.2	20	19.8
50	178	287	2.61	750	24	1.34	40	20	40.6	100	114	292	3.1	914	32	0.6	43.2	20	18.5
51	160	346	2.75	952	37	0.72	42	20	60.3	101	229	146	3.1	457	60	0.6	43.2	20	29
52	160	346	3.32	1149	43	1.1	42	20	45.1	102	229	146	3.1	457	32	0.6	43.2	20	37.3
53	160	325	3.54	1151	34	1.54	42	20	47.8	103	229	146	3.1	457	32	0.6	43.2	20	26.7
54	130	310	3.06	949	37	0.72	120	20	48.5	104	457	880	3.1	2743	30	1.2	41	20	246.2
55	130	310	3.71	1150	43	1.1	120	20	51	105	457	880	3.1	2743	31	1.2	41	20	238.2
56	130	310	3.71	1150	34	1.54	120	20	57.9	106	114	292	3.1	914	41	1.21	48.2	20	22.6
57	305	158	4.5	710	29	0.73	40	20	27.8	107	114	292	3.1	914	41	1.21	48.2	20	21.2
58	305	158	5.8	913	30	0.73	40	20	29.6	108	229	146	3.1	457	41	1.2	48.2	20	33.4
59	305	158	5.8	913	27	0.73	40	20	30.5	109	229	146	3.1	457	41	1.2	48.2	20	32.9
60	150	210	3.65	767	38	1.31	45	20	27.2	110	150	180	5.6	1000	20	0.87	115	20	19.1
61	150	210	3.65	767	33	1.36	45	20	22.7	111	150	180	5.6	1000	20	1.46	115	20	24.4
62	450	937	3.26	3050	46	0.51	37	20	142.3	112	150	180	5.6	1000	27	0.87	115	20	26.2
63	450	438	3.48	1525	35	0.55	37	20	87.8	113	150	180	5.6	1000	27	1.46	115	20	27.5
64	450	194	3.93	762	35	0.66	37	20	55.1	114	250	305	2.5	763	39	0.84	48	20	62.8
65	450	857	3.56	3050	36	2.23	37	20	240.3	115	250	305	3.5	1068	39	0.84	48	20	45.9
66	450	405	3.77	1525	35	2.36	37	20	140.3	116	250	310	2.5	775	33	0.42	144	20	79
67	450	188	4.05	762	35	2.54	37	20	74.6	117	250	310	3.5	1085	33	0.42	144	20	61.1
68	200	220	2.5	550	30	0.32	146.2	20	35.4	118	250	440	2.5	1100	43	0.89	48	20	132.5
69	150	220	2.5	550	30	0.43	146.2	20	25	119	300	584	2.5	1460	36	0.91	48	20	118.1
70	150	220	2.5	550	30	0.77	147.9	20	26.1	120	250	442	2.5	1105	72	1.46	48.2	20	119.2
71	200	220	3.5	770	30	0.32	146.2	20	29.4	121	300	578	2.5	1445	72	1.51	48.2	20	160.5
72	150	220	3.5	770	30	0.43	146.2	20	26.9	122	250	460	2.5	1150	41	0.44	144	20	67.6
73	150	220	3.5	770	30	0.77	147.9	20	29.6	123	300	594	2.5	1485	36	0.43	144	20	143.7
74	200	220	4.5	990	30	0.32	146.2	20	26.6	124	250	449	2.5	1123	72	0.82	144	20	103.5
75	150	220	4.5	990	30	0.43	146.2	20	24.6	125	300	594	2.5	1485	72	0.73	144	20	151.3
76	150	220	4.5	990	30	0.77	147.9	20	28.1	126	250	296	2.5	740	36	1.41	46.3	20	67.3

ID	$b_w$ (mm)	$d$ (mm)	$a/d$	$a$ (mm)	$f_c'$ (MPa)	$\rho_l$ (%)	$E_f$ (GPa)	$E_c$ (MPa)	$V$ (kN)	ID	$b_w$ (mm)	$d$ (mm)	$a/d$	$a$ (mm)	$f_c'$ (MPa)	$\rho_l$ (%)	$E_f$ (GPa)	$E_c$ (MPa)	$V$ (kN)
127	250	296	2.5	740	36	1.41	46.3	20	72.7	177	400	250	6	1500	50	1.71	47.5	20	91.1
128	250	455	2.5	1138	41	0.35	46.3	20	71.1	178	400	250	8	2000	48	2.28	47.5	20	84.8
129	250	434	2.5	1085	41	1.46	46.3	20	95.3	179	400	250	3	750	51	4.05	51.9	20	136.1
130	250	310	2.5	775	41	0.18	144	20	60.5	180	400	250	8	2000	48	4.05	51.9	20	99.8
131	250	310	2.5	775	41	0.66	144	20	74.3	181	200	250	4	1000	31	0.68	41.3	20	24.5
132	250	460	2.5	1150	41	0.22	144	20	73.3	182	200	250	4	1000	31	0.79	41.3	20	26.6
133	250	439	2.5	1098	41	0.65	144	20	85.6	183	200	250	4	1000	31	1.08	41.3	20	33.4
134	250	291	2.5	728	63	0.87	46.3	20	77.4	184	200	250	3	750	35	0.51	41.3	20	30.5
135	250	291	2.5	728	85	0.87	46.3	20	82	185	200	250	3	750	35	0.76	41.3	20	39.9
136	250	310	2.5	775	63	0.42	144	20	73.4	186	200	250	3	750	35	1.01	41.3	20	37.8
137	300	150	4	600	23	1.34	29	20	33.5	187	200	370	2.7	1000	22	0.12	141	20	34.7
138	300	150	4	600	28	1.79	29	20	36.5	188	200	370	2.7	1000	22	0.24	141	20	37.9
139	154	222	3.15	699	39	1.55	34	20	39.7	189	200	270	3.6	1000	29	0.16	141	20	34.2
140	635	202	6.04	1220	72	0.94	43.3	20	138.4	190	200	270	3.6	1000	29	0.33	141	20	34.2
141	635	202	6.04	1220	87	0.94	43.3	20	136.6	191	200	170	5.9	1000	24	0.26	141	20	18.5
142	635	202	6.04	1220	60	0.94	43.3	20	125	192	200	170	5.9	1000	24	0.52	141	20	21.7
143	635	202	6.04	1220	63	0.94	43.3	20	113.9	193	1000	140	6.07	850	48	1.01	41	20	100.6
144	635	202	6.04	1220	75	0.94	43.3	20	104.1	194	1000	140	6.07	850	48	0.79	47.6	20	125.1
145	635	202	6.04	1220	60	0.94	43.3	20	104.6	195	1000	140	6.07	850	48	1.01	47.6	20	112.1
146	635	227	4.47	1015	68	0.94	43.3	20	124	196	1000	140	6.07	850	48	1.22	47.6	20	125.1
147	635	240	6.04	1450	79	0.79	43.3	20	109	197	1000	140	6.07	850	50	1.42	47.6	20	170
148	635	240	6.04	1450	61	0.79	43.3	20	126.4	198	1000	137.5	6.18	850	48	1.85	51.9	20	151.8
149	635	240	6.04	1450	63	0.79	43.3	20	101	199	1000	140	6.07	850	43	1.01	69.5	20	174.6
150	635	240	6.04	1450	67	0.79	43.3	20	106.8	200	1000	140	6.07	850	49	1.21	69.5	20	128.1
151	1854	202	6.04	1220	84	0.96	43.3	20	396.3	201	1000	140	6.07	850	49	2.43	69.5	20	126.6
152	1854	202	6.04	1220	59	0.96	43.3	20	330	202	1000	137.5	6.18	850	50	2.55	69.5	20	127.6
153	1854	202	6.04	1220	63	0.96	43.3	20	279.3	203	1000	140	6.07	850	77	1.01	69.5	20	161.3
154	1854	202	6.04	1220	63	0.96	43.3	20	294.9	204	1000	140	6.07	850	83	1.03	69.5	20	143.7
155	1854	202	6.04	1220	57	0.96	43.3	20	303.8	205	1000	143.5	5.92	850	50	0.45	144	20	173.9
156	1854	202	6.04	1220	56	0.96	43.3	20	307.3	206	1000	143.5	5.92	850	50	0.54	144	20	147.6
157	1854	202	6.04	1220	84	0.54	43.3	20	282.9	207	1000	143.5	5.92	850	52	0.63	144	20	165.6
158	1854	202	6.04	1220	63	0.54	43.3	20	254	208	1000	143.5	5.92	850	45	0.72	144	20	163.6
159	1854	202	6.04	1220	56	0.54	43.3	20	225.9	209	1000	143.5	5.96	855	46	0.84	140	20	179.6
160	300	200	3.5	700	52	0.35	114	20	64.6	210	1000	143.5	5.96	855	49	0.98	140	20	192.6
161	300	300	3.5	1050	52	0.32	114	20	62.3	211	1000	143.5	5.96	855	41	1.11	140	20	198.6
162	300	400	3.5	1400	52	0.3	114	20	57.3	212	1000	143.5	5.92	850	76	0.63	144	20	174.6
163	300	500	3.5	1750	52	0.28	114	20	71.5	213	1000	143.5	5.92	850	86	0.63	144	20	219.4
164	300	400	6.5	2600	52	0.3	114	20	55.2	214	203	225	4.06	914	80	1.25	40.3	20	38.9
165	300	400	6	2400	52	0.3	114	20	65.9	215	152	225	4.06	914	80	1.66	40.3	20	33.2
166	150	280	2.5	700	45	0.11	148	20	23.2	216	165	225	4.06	914	80	2.1	40.3	20	36.5
167	150	280	5	1400	49	0.11	148	20	13.6	217	203	224	4.06	914	80	2.56	40.3	20	47.3
168	150	280	2.5	700	46	0.21	148	20	28.2	218	127	143	6.36	909	60	0.33	139	20	14.3
169	150	280	2.5	700	24	0.11	148	20	23.2	219	159	141	6.45	909	62	0.58	139	20	20.3
170	400	250	3	750	51	0.57	47.5	20	57.1	220	89	143	6.36	909	81	0.47	139	20	10
171	400	250	3	750	49	0.86	47.5	20	75.1	221	121	141	6.45	909	81	0.76	139	20	15.7
172	400	250	3	750	51	1.14	47.5	20	86.1	222	150	250	3	750	28	0.55	94	20	38.3
173	400	250	3	750	51	1.71	47.5	20	109.1	223	150	250	3	750	33	1.1	94	20	43.8
174	400	250	3	750	52	2.28	47.5	20	116.1	224	150	250	3	750	31	1.39	94	20	48.3
175	400	250	3	750	50	0.86	47.5	20	79.1	225	150	250	3	750	35	2.2	94	20	59.1
176	400	250	4	1000	51	1.14	47.5	20	90.4	226	150	250	2.5	625	34	1.04	100	20	38.8

ID	$b_w$ (mm)	d (mm)	$a/d$	a (mm)	$f'_c$ (MPa)	$\rho_l$ (%)	$E_f$ (GPa)	$E_c$ (MPa)	V (kN)
227	300	500	2.5	1250	30	1.04	100	20	145.4
228	150	170	4.12	700	24	0.92	45.8	20	12.7
229	150	170	4.12	700	24	1.54	45.8	20	13.6
230	150	170	4.12	700	31	0.92	45.8	20	14.1
231	150	170	4.12	700	31	1.54	45.8	20	15.3
232	300	441	3.02	1330	42	3.65	62.6	20	145.4
233	300	412	3.16	1300	43	3.25	44	20	153.9
234	300	404	3.71	1500	28	3.98	62.6	20	107.6
235	420	83	3.61	300	61	0.61	42	20	19.9
236	420	82	6.1	500	61	1.1	42	20	25.5
237	420	80	6.25	500	61	1.77	40	20	32
238	420	78	6.41	500	61	2.61	40	20	40.5
239	420	83	3.61	300	74	0.61	42	20	24.9
240	420	82	6.1	500	74	1.1	42	20	22
241	420	80	6.25	500	74	1.77	40	20	32
242	420	78	6.41	500	74	2.61	40	20	36.5
243	420	83	3.61	300	93	0.61	42	20	35.9
244	420	82	6.1	500	93	1.1	42	20	23
245	420	80	6.25	500	93	1.77	40	20	32
246	420	78	6.41	500	93	2.61	40	20	38.5
247	420	75	6	450	48	0.68	42	20	24.8
248	420	73	6.16	450	48	0.93	42	20	27.6
249	420	73	6.16	450	48	1.16	42	20	29.6
250	420	75	6	450	76	0.68	42	20	27.5
251	420	73	6.16	450	76	0.93	42	20	26.5
252	420	73	6.16	450	76	1.16	42	20	31.4
253	420	75	6	450	92	0.68	42	20	23.7
254	420	73	6.16	450	92	0.93	42	20	25.7
255	420	73	6.16	450	92	1.16	42	20	34.5
256	150	270	4.07	1100	60	0.39	70	20	19.8
257	150	270	4.07	1100	60	0.51	70	20	23
258	200	270	2.5	675	47	1.82	64	20	82.1
259	200	270	2.5	675	47	2.23	64	20	75.7
260	200	270	2.5	675	47	2.51	64	20	63.1
261	400	575	2.92	1680	32	1	61.2	20	159.5
262	400	575	2.92	1680	40	1	71.2	20	169
263	400	575	2.92	1680	102	1	61.2	20	166
264	600	262	6.68	1750	58	0.76	55.4	20	89.2
265	600	262	6.68	1750	58	1.51	55.4	20	116.2
266	1200	180	5.8	1050	33	0.66	44	20	140.7
267	1200	180	5.8	1050	33	0.88	44	20	151.7
268	1200	180	5.8	1050	33	1.1	44	20	158.7
269	1200	180	5.8	1050	33	0.33	50	20	102.8
270	1200	180	5.8	1050	33	0.44	50	20	133.1
271	1200	180	5.8	1050	33	0.57	50	20	166.6
272	152	220	3.3	725	49	0.3	50	20	17.4
273	152	220	3.3	725	49	0.47	50	20	23.5
274	152	220	3.3	725	49	0.68	50	20	19

ID	$b_w$ (mm)	d (mm)	$a/d$	a (mm)	$f'_c$ (MPa)	$\rho_l$ (%)	$E_f$ (GPa)	$E_c$ (MPa)	V (kN)
275	152	220	3.3	725	49	0.94	50	20	28.4
276	152	220	3.3	725	49	1.35	50	20	30.4
277	152	220	2.5	550	49	0.3	50	20	20
278	152	220	2.5	550	49	0.47	50	20	32.1
279	152	220	2.5	550	49	0.68	50	20	27.5
280	200	170	5.56	945	36	1.21	53	20	30.9
281	200	170	5.56	945	36	2	51	20	40.3
282	200	170	5.56	945	36	3.09	51	20	46.8
283	200	170	7	1190	36	3.74	51	20	41.6
284	200	165	7	1155	36	4.64	48	20	49.8
285	200	165	7	1155	36	6.18	48	20	52.9
286	100	180	5.56	1000	41	0.74	40.8	20	10.2
287	100	180	5.56	1000	41	1.48	40.8	20	12.3
288	100	180	5.56	1000	66	0.35	124	20	9.1
289	100	180	5.56	1000	66	0.71	124	20	14.2
290	150	379	2.9	1100	31	0.99	51.5	20	35.3
291	150	377	2.92	1100	33	1.07	51.5	20	32.8
292	150	376	2.93	1100	33	1.35	51.5	20	39.6
293	150	377	2.92	1100	31	1.42	51.5	20	35.8
294	150	376	2.93	1100	33	1.8	51.5	20	39.2
295	150	368	2.99	1100	31	1.02	51.5	20	35.8
296	150	367	3	1100	33	1.85	51.5	20	48.8
297	100	566	3.53	2000	34	8.52	59	20	131.8
298	100	566	3.53	2000	80	11.36	59	20	189.8
299	100	572	3.5	2000	43	8.43	59	20	141.8
300	100	561	3.57	2000	75	11.46	62.6	20	210.8
301	100	572	3.5	2000	37	8.43	62.6	20	127.8
302	110	195	2.5	488	35	0.66	124	20	19.7
303	200	236.2	3.05	720	35	2.1	62.6	20	63.9

**Author contributions** T-HN: conceptualization, software, visualization, writing—original draft. X-BN: methodology, data curation, writing—original draft. V-HN: validation; visualization. T-HTN: validation; visualization. D-DN: methodology, formal analysis, writing—original draft, writing—review and editing, supervision.

**Funding** No funding was used in this study.

**Data availability** The data used to support the findings of this study are included in the article.

## Declarations

**Conflict of interest** The authors declare that they have no known competing financial interests or personal relationships that could have appeared to influence the work reported in this paper.

## References

- AASHTO, L. (2009). *Bridge design guide specifications for GFRP-reinforced concrete bridge decks and traffic railings*. The American Association of State Highway and Transportation Officials.
- ACI. (2015). *ACI 440.1 R-15: Guide for the design & construction of structural concrete reinforced with FRP bars*. American Concrete Institute.
- Ahmed, A., Elkhatatny, S., Ali, A., Mahmoud, M., & Abdulraheem, A. (2019). New model for pore pressure prediction while drilling using artificial neural networks. *Arabian Journal for Science and Engineering*, 44, 6079–6088. <https://doi.org/10.1007/s13369-018-3574-7>
- Askar, M. K., Hassan, A. F., & Al-Kamaki, Y. S. (2022). Flexural and shear strengthening of reinforced concrete beams using FRP composites: A state of the art. *Case Studies in Construction Materials*, 17, e01189.
- Asteris, P. G., and Mokos, V. G. (2019). Concrete compressive strength using artificial neural networks. *Neural Computing and Applications*, 32(15), 11807–11826.
- Bentz, E. C., Massam, L., & Collins, M. P. (2010). Shear strength of large concrete members with FRP reinforcement. *Journal of Composites for Construction*, 14, 637–646.
- BISE. (1999). *Interim guidance on the design of reinforced concrete structures using fiber composite reinforcement*. British Institution of Structural Engineers Seto Ltd.
- Burden, F., & Winkler, D. (2009). Bayesian regularization of neural networks. In: D. J. Livingstone (Ed.), *Artificial neural networks. Methods in molecular biology™*, vol 458. Humana Press. [https://doi.org/10.1007/978-1-60327-101-1\\_3](https://doi.org/10.1007/978-1-60327-101-1_3)
- CNR-DT203. (2007). *Guide for the design and construction of concrete structures reinforced with fiber-reinforced polymer bars*. Advisory Committee on Technical Recommendations for Construction.
- CSA. (2012). *S806-12: Design & construction of building structures with fibre reinforced polymers*. Canadian Standards Association.
- Deitz, D., Harik, I., & Gesund, H. (1999). One-way slabs reinforced with glass fiber reinforced polymer reinforcing bars. *Special Publication*, 188, 279–286.
- Eberhart, R., & Kennedy, J. (1995). *Particle swarm optimization* (pp. 1942–1948). Citeseer.
- El-Sayed, A. K., El-Salakawy, E. F., & Benmokrane, B. (2006). Shear strength of FRP-reinforced concrete beams without transverse reinforcement. *ACI Materials Journal*, 103, 235.
- Foresee, F. D., & Hagan, M. T. (1997). Gauss-Newton approximation to Bayesian learning. In: *IEEE*, pp. 1930–1935.
- Hoult, N., Sherwood, E., Bentz, E. C., & Collins, M. P. (2008). Does the use of FRP reinforcement change the one-way shear behavior of reinforced concrete slabs? *Journal of Composites for Construction*, 12, 125–133.
- ISIS-M03. (2007). *Reinforcing concrete structures with fiber reinforced polymers*. Canadian network of Centers of Excellence on Intelligent Sensing for Innovative Structures, University of Winnipeg.
- JSCE. (1997). *Recommendation for design and construction of concrete structures using continuous fiber reinforcing materials* (Vol. 23). Japan Society of Civil Engineers, Concrete Engineering Series.
- Jumaa, G. B., & Yousif, A. R. (2018). Predicting shear capacity of FRP-reinforced concrete beams without stirrups by artificial neural networks, gene expression programming, and regression analysis. *Advances in Civil Engineering*, 2018, 1–16.
- Kara, I. F. (2011). Prediction of shear strength of FRP-reinforced concrete beams without stirrups based on genetic programming. *Advances in Engineering Software*, 42, 295–304.
- Kaveh, A., & Bondarabady, H. R. (2004). Wavefront reduction using graphs, neural networks and genetic algorithm. *International Journal for Numerical Methods in Engineering*, 60, 1803–1815.
- Kaveh, A., Gholipour, Y., & Rahami, H. (2008). Optimal design of transmission towers using genetic algorithm and neural networks. *International Journal of Space Structures*, 23, 1–19.
- Kaveh, A., & Khalegi, A. (1998). Prediction of strength for concrete specimens using artificial neural networks. In B. H. V. Topping (Ed.), *Advances in engineering computational technology* (pp. 165–171). Edinburgh, UK: Civil-Comp Press, <https://doi.org/10.4203/ccp.53.4.3>.
- Kaveh, A., & Khavaninzadeh, N. (2023). *Efficient training of two ANNs using four meta-heuristic algorithms for predicting the FRP strength* (pp. 256–272). Elsevier.
- Kaveh, A., & Servati, H. (2001). Design of double layer grids using backpropagation neural networks. *Computers & Structures*, 79, 1561–1568.
- Mai, S. H., Tran, V.-L., Nguyen, D.-D., Nguyen, V. T., & Thai, D.-K. (2022). Patch loading resistance prediction of steel plate girders using a deep artificial neural network and an interior-point algorithm. *Steel and Composite Structures*, 45, 159.
- Marani, A., & Nehdi, M. L. (2022). Predicting shear strength of FRP-reinforced concrete beams using novel synthetic data driven deep learning. *Engineering Structures*, 257, 114083.
- Michaluk, C. R., Rizkalla, S. H., Tadros, G., & Benmokrane, B. (1998). Flexural behavior of one-way concrete slabs reinforced by fiber reinforced plastic reinforcements. *Structural Journal*, 95, 353–365.
- Naderpour, H., Pouraeidi, O., & Ahmadi, M. (2018). Shear resistance prediction of concrete beams reinforced by FRP bars using artificial neural networks. *Measurement*, 126, 299–308.
- Nehdi, M., El Chabib, H., & Saïd, A. A. (2007). Proposed shear design equations for FRP-reinforced concrete beams based on genetic algorithms approach. *Journal of Materials in Civil Engineering*, 19, 1033–1042.
- Nguyen, D.-D., Tran, V.-L., Ha, D.-H., Nguyen, V.-Q., & Lee, T.-H. (2021a). *A machine learning-based formulation for predicting shear capacity of squat flanged RC walls* (pp. 1734–1747). Elsevier.
- Nguyen, T.-H., Tran, N.-L., & Nguyen, D.-D. (2021b). Prediction of axial compression capacity of cold-formed steel oval hollow section columns using ANN and ANFIS models. *International Journal of Steel Structures*. <https://doi.org/10.1007/s13296-021-00557-z>
- Nguyen, T.-H., Tran, N.-L., & Nguyen, D.-D. (2021c). Prediction of critical buckling load of web tapered I-section steel columns using artificial neural networks. *International Journal of Steel Structures*, 21(4), 1159–1181.
- Nguyen, T.-H., Tran, N.-L., Phan, V.-T., & Nguyen, D.-D. (2023a). Improving axial load-carrying capacity prediction of concrete columns reinforced with longitudinal FRP bars using hybrid GA-ANN model. *Asian Journal of Civil Engineering*, 1–11. <https://doi.org/10.1007/s42107-023-00695-1>
- Nguyen, T.-H., Tran, N.-L., Phan, V.-T., & Nguyen, D.-D. (2023b). Prediction of shear capacity of RC beams strengthened with FRCM composite using hybrid ANN-PSO model. *Case Studies in Construction Materials*, 18, e02183.
- Nguyen, V.-Q., Tran, V.-L., Nguyen, D.-D., Sadiq, S., & Park, D. (2022). Novel hybrid MFO-XGBoost model for predicting the racking ratio of the rectangular tunnels subjected to seismic loading. *Transportation Geotechnics*, 37, 100878.
- Nikoo, M., Aminnejad, B., & Lork, A. (2021). Predicting shear strength in FRP-reinforced concrete beams using bat algorithm-based artificial neural network. *Advances in Materials Science and Engineering*, 2021, 1–13.
- Peng, F., Xue, W., & Xue, W. (2020). Database evaluation of shear strength of slender fiber-reinforced polymer-reinforced concrete members. *ACI Structural Journal*, 117, 273–281.

- Rönnholm, M., Arve, K., Eränen, K., Klingstedt, F., Salmi, T., & Saxén, H. (2005). ANN modeling applied to NO X reduction with octane. In B. Ribeiro, R. F. Albrecht, A. Dobnikar, D. W. Pearson, & N. C. Steele (Eds.), *Adaptive and Natural Computing Algorithms* (pp. 100–103). Springer. [https://doi.org/10.1007/3-211-27389-1\\_24](https://doi.org/10.1007/3-211-27389-1_24)
- Selvan, S. S., Pandian, P. S., Subathira, A., & Saravanan, S. (2018). Comparison of response surface methodology (RSM) and artificial neural network (ANN) in optimization of aegle marmelos oil extraction for biodiesel production. *Arabian Journal for Science and Engineering*, 43, 6119–6131. <https://doi.org/10.1007/s13369-018-3272-5>
- Shehata, E. F. (1999). *Fibre-reinforced polymer (FRP) for shear reinforcement in concrete structures*. Ph.D. dissertation (University of Manitoba, Winnipeg, Canada).
- Simon, D. (2013). *Evolutionary optimization algorithms*. Wiley.
- Sivanandam, S., Deepa, S., Sivanandam, S., & Deepa, S. (2008). *Genetic algorithms*. Springer.
- Tottori, S., & Wakui, H. (1993). Shear capacity of RC and PC beams using FRP reinforcement. *Special Publication*, 138, 615–632.
- Tran, N.-L., Nguyen, D.-D., & Nguyen, T.-H. (2022). Prediction of speed limit of cars moving on corroded steel girder bridges using artificial neural networks. *Sādhanā*, 47, 1–14.
- Tran, V.-L., & Kim, S.-E. (2020). Efficiency of three advanced data-driven models for predicting axial compression capacity of CFDST columns. *Thin-Walled Structures*, 152, 106744. <https://doi.org/10.1016/j.tws.2020.106744>
- Tran, V.-L., & Nguyen, D.-D. (2022). Novel hybrid WOA-GBM model for patch loading resistance prediction of longitudinally stiffened steel plate girders. *Thin-Walled Structures*, 177, 109424.
- Tureyen, A. K., & Frosch, R. J. (2002). Shear tests of FRP-reinforced concrete beams without stirrups. *Structural Journal*, 99, 427–434.
- Vakhshouri, B., & Nejadi, S. (2018). Prediction of compressive strength of self-compacting concrete by ANFIS models. *Neurocomputing*, 280, 13–22. <https://doi.org/10.1016/j.neucom.2017.09.099>
- Wakjira, T. G., Al-Hamrani, A., Ebead, U., & Alnahhal, W. (2022). Shear capacity prediction of FRP-RC beams using single and ensemble ExPlainable Machine learning models. *Composite Structures*, 287, 115381.
- Xue, W., Peng, F., & Zheng, Q. (2016). Design equations for flexural capacity of concrete beams reinforced with glass fiber-reinforced polymer bars. *Journal of Composites for Construction*, 20, 04015069.

**Publisher's Note** Springer Nature remains neutral with regard to jurisdictional claims in published maps and institutional affiliations.

Springer Nature or its licensor (e.g. a society or other partner) holds exclusive rights to this article under a publishing agreement with the author(s) or other rightsholder(s); author self-archiving of the accepted manuscript version of this article is solely governed by the terms of such publishing agreement and applicable law.